ACS Catalysis

Research Article

Cite This: ACS Catal. 2018, 8, 10096−10110

pubs.acs.org/acscatalysis

Catalytic Mechanism of the Serine Hydroxymethyltransferase: A Computational ONIOM QM/MM Study

Henrique S. Fernandes,[§] Maria João Ramos, and Nuno M. F. S. A. Cerqueira*[,§]

UCIBIO@REQUIMTE, Departamento de Química e Bioquímica, Faculdade de Ciências da Universidade do Porto, Rua do Campo Alegre s/n, 4169-007 Porto, Portugal

Supporting Information

ABSTRACT: Serine hydroxymethyltransferase (SHMT) is an important drug target to fight malaria, which is one of the most devastating infectious diseases, with 216 million cases cited and accounting for ∼450 000 deaths in 2016. In this paper, computational studies were performed to unveil the catalytic mechanism of SHMT using quantum mechanics/molecular mechanics (QM/MM) methodologies. This enzyme is responsible for the extraordinary cyclization of a tetrahydrofolate (THF) into 5,10-methylene−THF. This process is catalyzed by a pyridoxal-5′-phosphate (PLP) cofactor that binds L-serine and, from this, one molecule of L-glycine is produced. The results show that the catalytic process occurs in eight sequential steps that involve an α-elimination, the cyclization of the 5-hydroxymethyl−THF intermediate into 5,10-methylene−THF, and the protonation of the quinonoid intermediate. According to the calculated energetic profile, the rate-limiting step of the full mechanism is the elimination of the hydroxymethyl group, from which results a formaldehyde intermediate that then becomes covalently bonded to the THF cofactor. The calculated barrier (DLPNO−CCSD(T)/CBS:ff99SB) for the rate-limiting step (18.0 kcal/mol) agrees very well with the experimental kinetic results (15.7−16.2 kcal/mol). The results also highlight the key role played by Glu57 during the full catalytic process and particularly in the first step of the mechanism that requires an anionic Glu57, contrasting with some proposals available in the literature for this step. It was also concluded that the cyclization of THF must occur in the enzyme, rather than in solution, as it has been proposed also in the past. Together, all of these results provide knowledge and insight on the catalytic mechanism of SHMT, which can now be used to develop inhibitors targeting SHMT and, therefore, antimalaria drugs.

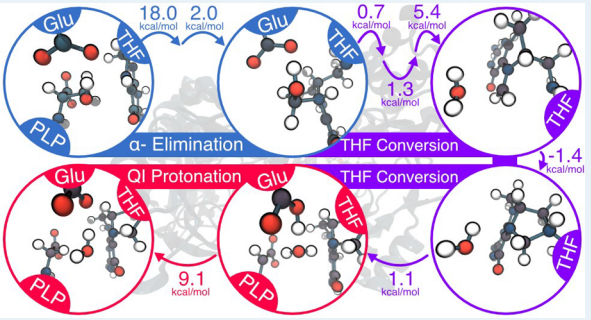

KEYWORDS: *serine hydroxymethyltransferase (SHMT), malaria, tetrahydrofolate (THF), pyridoxal-5′-phosphate (PLP), serine, catalytic mechanism, ONIOM, QM/MM*

1. INTRODUCTION

Malaria is one of the most devastating infectious diseases; it is caused by a parasitic infection transmitted by mosquitoes. According to the last World Health Organisation (WHO) report, 216 million new cases of malaria and ∼450 000 deaths were caused by this disease in 2016. Despite the resources and investments allocated to find a universal cure for this disease (2.7 billion dollars in 2016), the control and eventual elimination of malaria is seriously questioned, because of the resistance of parasites to antimalarial drugs. This effect has become even more dramatic in five countries of the Greater Mekong Subregion and at the Cambodia−Thailand border, where *Plasmodium falciparum*—the species that causes the deadliest form of malaria[1]—has become resistant to the major antimalarial drugs used clinically.[1,2]

Together, all of these facts demand an urgent need for new drug targets, which can be used to design new and more efficient therapeutics against the malaria pathogen. Particular attention is being given to those that provide a selective interference with the parasite metabolism without harming the human host.[1,3,4] In this regard, some of the most promising targets are enzymes involved in the *de novo* purine biosynthesis in the malaria parasites, such as serine hydroxymethyltransferase (SHMT).[5−8]

The SHMT (EC 2.1.2.1) is a pyridoxal-5′-phosphate (PLP)-dependent enzyme that catalyzes the reversible transfer of a carbon-unit from the L-serine to a second cofactor, the tetrahydrofolate (THF) (see Figure 1). At the end of the reaction, a glycine molecule is released as well as a 5,10-methylene−THF molecule, which is a precursor in the synthesis of purines and thymidylate.[9] Since the purines biosynthesis is vital for the pathogen survival (synthesis of nucleic acids), the inhibition of SHMT has been noted as an important drug target for malaria.[5] Furthermore, the comparison between the tridimensional structure of the human and *P. falciparum* forms of the SHMT revealed key

Received: June 14, 2018
Revised: September 3, 2018
Published: September 18, 2018

DOI: 10.1021/acscatal.8b02321
ACS Catal. 2018, 8, 10096−10110

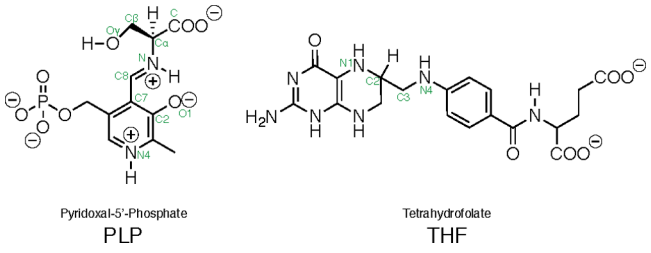

Figure 1. Structure of the external aldimine (pyridoxal-5′-phosphate + L-serine) (left) and the tetrahydrofolate (THF) cofactor (right).

differences that can help to rationalize the specific synthesis of new inhibitors for the *P. falciparum* form of the SHMT.[10]

Despite the importance that SHMT has gathered in the last two years, this enzyme continues to be poorly understood. This happens due to the complex chemistry that it catalyzes, which requires the participation of two cofactors (PLP and THF) and the multisequential steps required for the cyclization of the THF into the final product, 5,10-methylene−THF. This knowledge is very important, since it will provide clues about the enzymatic activity and how it can be inhibited. This information can then be used to develop new inhibitors targeting this enzyme with potential application as new antimalaria drugs.

Since SHMT is a PLP-dependent enzyme, the catalytic activity of this enzyme is composed of three stages. The first two stages are common to all PLP-dependent enzymes and were already studied.[11,12] The first stage involves the activation of the enzyme, in which the PLP cofactor becomes covalently bonded to an active site Lys residue and forms what is commonly known as the internal aldimine. The second stage is triggered when the substrate is available, and it becomes covalently bonded to the PLP cofactor, forming the external aldimine. The third stage is what differentiates the PLP-dependent enzymes, and it is specific to each class of enzymes. In the case of SHMT, the enzyme catalyzes an α-elimination of L-Ser that is subsequently inserted into the THF cofactor. (See Figure 2.)

The experimental kinetic data available for the *E. coli* form of the SHMT indicates an activation barrier limit of 15.7−16.2 kcal/mol, based on the available k_{cat} values of 686.6 ± 21.7 min^{-1} (pH 7.2, 20 °C)[13] and 790 min^{-1} (pH 7.2, 30 °C).[14]

Currently, there is no accepted mechanism for the α-elimination catalyzed by SHMT, and only two hypotheses are available in the literature. They diverge in the way through

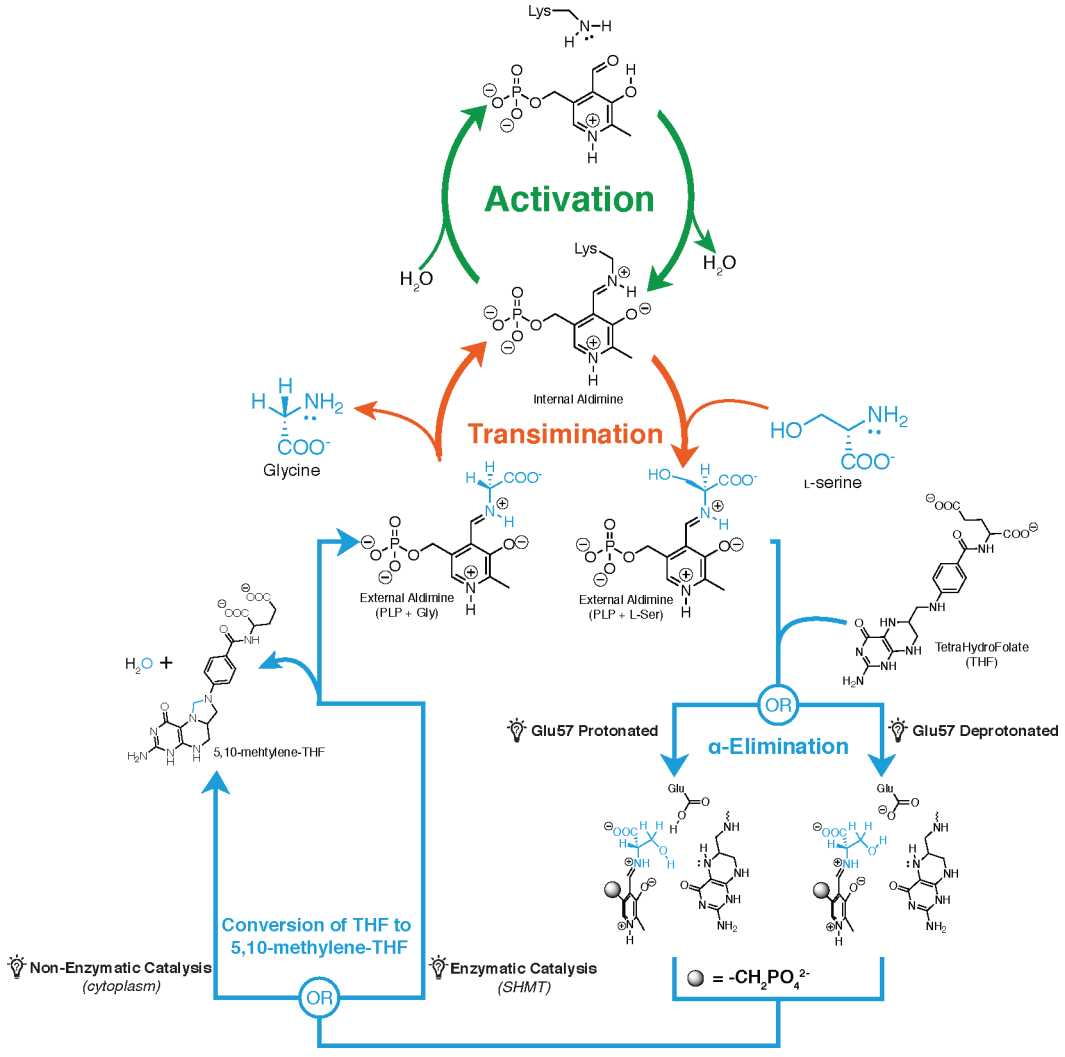

Figure 2. Scheme representing the mechanism behind the internal and external aldimine formation for PLP-dependent enzymes and the specific α-elimination reaction.

DOI: 10.1021/acscatal.8b02321
ACS Catal. 2018, 8, 10096−10110

which the hydroxymethyl group is transferred from L-serine, which is bonded to the PLP cofactor and form an external aldimine, to THF. One of the hypothesis suggests that the reaction occurs in one step, where nitrogen N1 of THF makes a nucleophilic attack on the Cβ of the L-Ser promoting the α-elimination reaction. In the other hypothesis, the reaction requires two steps. The first step involves the formation of a formaldehyde molecule (through the dissociation of the hydroxymethyl group from the external aldimine), which then undergoes a nucleophilic attack from nitrogen N1 of the THF cofactor.[15] These two hypotheses also diverge regarding the protonation state of Glu57, which interacts very closely with the hydroxyl group of the external aldimine. In the first proposal, Glu57 is proposed to be protonated, whereas, in the second proposal, the mechanism requires an unprotonated Glu57.[15−17]

The role played by Glu57 in the reaction is known to be fundamental for catalysis, since several mutagenic studies have shown that its mutation by Gln, Leu, or Lys residues reduces the activity of the enzyme drastically (more than 300 times), but the role played by this residue in the mechanism continues to be poorly understood.[16,18]

Some authors also suggest that the reaction of the formaldehyde molecule with THF can occur in the solvent and not in the enzyme.[15,19] However, so far, no experimental result is currently available to provide insights into this hypothesis.

In this paper, the catalytic mechanism of the SHMT was studied employing computational means and using quantum mechanics/molecular mechanics (QM/MM) methodologies. Based on the mechanistic proposals available in the literature, and described above, two models of the enzyme were set up to assess the role of the protonation of the Glu57 residue in the catalytic mechanism and also to understand if the hydroxymethyl group is transferred directly to the THF cofactor or it involves the formation of a formaldehyde intermediate in an intermediate step. A third model was also built to study the possibility in which the cyclization of the THF intermediate occurs in the solvent and does not require the presence of the enzyme.

2. METHODOLOGY

2.1. Preparing the Structure. This study was conducted using the crystallographic structure of SHMT from *Escherichia coli* deposited in the Protein Data Bank (PDB) with the reference 1DFO.[17]

Although here, it was our intention to study the SHMT present in the *Plasmodium falciparum*, we have chosen to use the PDB from *Escherichia coli*, because this structure contains the external aldimine with the product of the reaction (PLP + Glycine) and an analogue of the first THF intermediate. This type of information is not available in the PDB file of SHMT from *P. falciparum* (PDB code: 4O6Z).[20] Although the identity between both proteins is not very high (43%; see Figure S1A in the Supporting Information) (BLASTP 2.8.0+),[21,22] the structure of both proteins (see Figure S1B in the Supporting Information) is very similar nearby, and the region of the active site can be almost overlapped (see Figure S1C in the Supporting Information).

The model system that was used in the computational studies includes one of the homodimers of SHMT that is present in the crystallographic structure with the PDB code 1DFO. The external aldimine (PLP+Gly) present on the PDB was used to model the quinonoid intermediate of the reaction, adding only one proton to the Cα carbon of the substrate. The 5-formyl−THF inhibitor was used as a template to build the 5-hydroxymethyl−THF intermediate that results from the transfer of the hydroxymethyl group during the first step of the reaction.

From this model, two additional models were built to accommodate different protonation states of Glu57: Model 1 and Model 2.

An additional model was built to study if the formation of the 5,10-methylene−THF could occur in a nonenzymatic process. This model (called Model 3) only contains the 5-hydroxymethyl−THF molecule that results from the reaction of the THF cofactor with the formaldehyde molecule (that occurs inside the enzyme). To model the solvent effect, an implicit solvent model was employed (water, ε = 78.3553) using the IEFPCM formalism integrated with Gaussian09.[23]

2.2. Structure Minimization. The protein, and the external aldimine (L-Ser bounded to the PLP cofactor), as well as the THF cofactor were solvated by using TIP3P[24]-type water molecules. The protein was placed inside a water box, so that each atom of the protein was distanced at least 12 Å from the faces. The SANDER software from the AMBER12 package was used to add the H atoms to the model.[25] The protonation states for all amino acids were predicted by PROPKA 3.1[26,27] at pH 7.0, except for the Glu57 residue, whose protonation state was tested in Models 1 and 2.

The parametrization of the 5-hydroxymethyl−THF and external aldimine was made by optimizing their structures using the Hartree−Fock (HF/6-31G(d)) method to obtain the atomic charges and the antechamber software from AMBER12 package[25] to assign the atom types. The *frcmod*, *prepc*, and *lib* files containing all the parameters and topology for the external aldimine and 5-hydroxymethyl−THF molecules are available in the Supporting Information (SI).

The geometry of the full system was minimized through four sequential steps using the AMBER12 package[25] and the GAFF[28] and ff99SB[29] force fields. First, we executed a minimization of all water molecules and, afterward, all of the H atoms. Subsequently, all atoms from the system, except backbone atoms, were minimized, and finally, a minimization of all system with no constraint was conducted.

2.3. QM/MM. The QM/MM model was built loading the minimized structure from the previous procedure, using the molUP plugin[30] for Visual Molecular Dynamics (VMD) software.[31] The QM/MM model included the full dimer, the two external aldimines, the two 5-hydroxymethyl−THF molecules, and a 5.0 Å coating of water molecules. It was created by following the general protocol that is widely accepted to study enzymatic mechanisms.[32]

The subtractive QM/MM model methodology ONIOM was used in all of the calculations.[33−35] This method allows a model system to be split into different regions that are computed by different theoretical levels. In this work, the system was divided into two regions: the high-level (HL) layer, which was calculated with density functional theory (DFT), and the low-level (LL) layer, which was calculated with molecular mechanics (MM).

The atoms included in the HL layer were adjusted from step to step, since different types of reactions occur during the full catalytic process. In the α-elimination reactions, the HL includes the atoms from the external aldimine, THF cofactor, and some active site residues that, in total, amounting to 106

DOI: 10.1021/acscatal.8b02321
ACS Catal. 2018, 8, 10096−10110

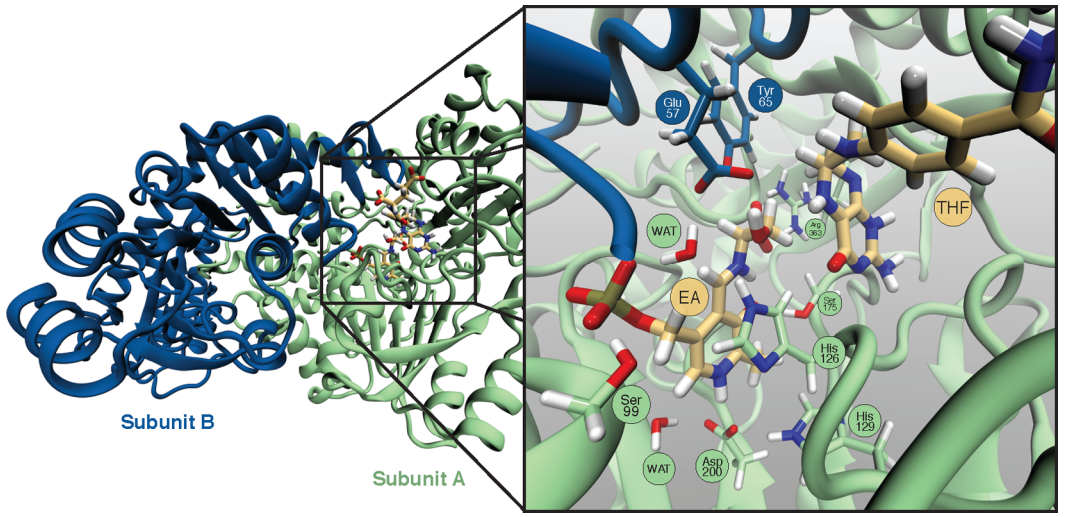

Figure 3. (Left) Structure of the SHMT dimer (green represents subunit A; blue represents subunit B) and licorice representation of the HL layer. (Right) The substrate, cofactors, and the active site residues are represented in licorice and colored according to the subunit to which they belong to (green represents subunit A; blue represents subunit B). Each molecule is identified by a circular tag.

atoms (Arg3643, Asp200, His129, Asn102, Glu57, Ser35, and a water molecule). In the study of the conversion of the THF intermediate to 5,10-methylene−THF, only the THF intermediate and the active site residue Glu57 were included in the HL layer, amounting to 85 atoms. In the last stage of the mechanism, a set of atoms similar to those used in the α-elimination was used (121 atoms in total). (See Figure 3.) The remaining atoms of the system were included in the LL layer. H atoms were used as link atoms to complete the valence of the bonds crossing between the two layers of the ONIOM QM/MM scheme.

The geometry optimization of the HL layer was performed using the B3LYP functional (DFT).[36] The B3LYP functional was selected because of its very good results in the study of similar biological systems.[37−44] The 6-31G(d,p) basis set was employed as available in Gaussian 09.[23]

We explored the reactional space through linear transit scans along the reaction coordinates implicated in each step of the reaction. Afterward, the transition states (TS) were optimized, using the structures of higher energy obtained with each linear scan. The reactant and product of each step were determined using internal reaction coordinate (IRC)[45] calculations. The TSs were confirmed by vibrational frequency calculations, resulting in a single imaginary frequency with the correct transition vectors assigned. The vibrational frequency calculations were also conducted for the minima, and no imaginary frequencies were observed. The zero point energy (ZPE), thermal, and entropic energy corrections were estimated at 310.15 K and 1.0 bar during the frequency calculation of TS and related minima structures.

Finally, the energies of all TS, reactant, and product were determined using DLPNO−CCSD(T)/CBS for the HL layer. The recent domain-based local pair natural orbital-coupled cluster method with single, double, and perturbative triple excitations (DLPNO−CCSD(T))[46,47] was employed, since it allows one to calculate energies that closely fit those obtained with the canonical method (CCSD(T)) at a much lower computational cost.[48,49] Moreover, several studies have already shown the application of this new method in several biochemistry areas.[50−52] For each minima and TS of each step, the HL layer was isolated to perform DLPNO−CCSD(T) single-point (SP) energy calculations using the ORCA software (version 4.0.1.2).[53] The SP energy calculations were performed using the cc-pVDZ[54] and cc-pVTZ[54] basis sets, and the cc-pVDZ/C[55,56] and cc-pVTZ/C[56] correlation fitting basis sets, respectively. The combination of the energies obtained with cc-pVDZ | cc-pVDZ/C and cc-pVTZ | cc-pVTZ/C basis sets for the HL layer were used to extrapolate to the complete basis set (CBS) limit, according to Truhlar's extrapolation approach,[57] except for the exponents α and β. The values of 4.42 and 2.46 were considered to correspond to exponents α and β, respectively, in the extrapolation, according to the ORCA documentation.

Concerning the interaction between the HL and LL layers, the mechanical embedding method was used to perform all of the calculations, because the electrostatic embedding scheme is computationally very expensive, considering the size of the system and the number of reactions studied in this work. The activation and reaction free energies presented here were determined by the difference between the Gibbs free energies of TS and reactant, or product and reactant, respectively.

All the preparation of the Gaussian 09[23] input files and subsequent results analysis were made using molUP plugin[30] for VMD software.[31]

The structures (PDB files) for the reactant, TS, and product of each step studied in this work are available in the Supporting Information (SI).

3. RESULTS AND DISCUSSION

The computational calculations regarding the catalytic mechanism of SHMT were divided into three main stages: (i) the first stage, which involved the α-elimination process; (ii) the second stage, which involved the conversion of the THF intermediate to 5,10-methylene−THF; and (iii) the third stage, which involved the protonation of the quinonoid intermediate (QI) and subsequent enzymatic turnover. Each of these stages is described and discussed in detail in the following sections of the manuscript. Each of these stages is described and discussed in detail in the following sections of the manuscript. The analysis of all key interactions for the minima and TS of each step is provided in Figure S3 in the SI.

DOI: 10.1021/acscatal.8b02321
ACS Catal. 2018, 8, 10096−10110

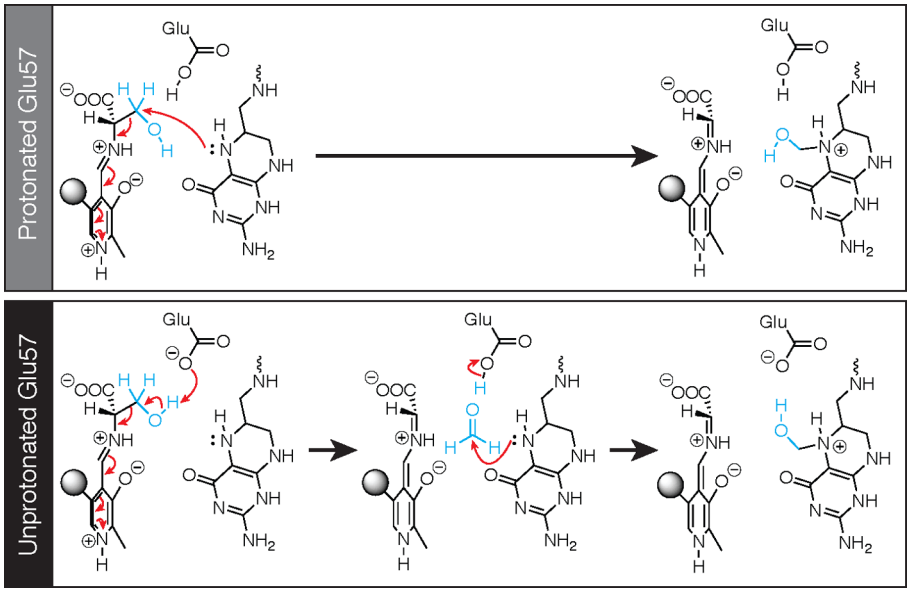

Figure 4. Schematic representation of the two mechanistic proposals for the α-elimination of L-serine that is bonded to the PLP cofactor and forms the external aldimine, considering different protonation states of Glu57: protonated (top) and unprotonated (bottom). The spheres represent the phosphate group of the PLP cofactor.

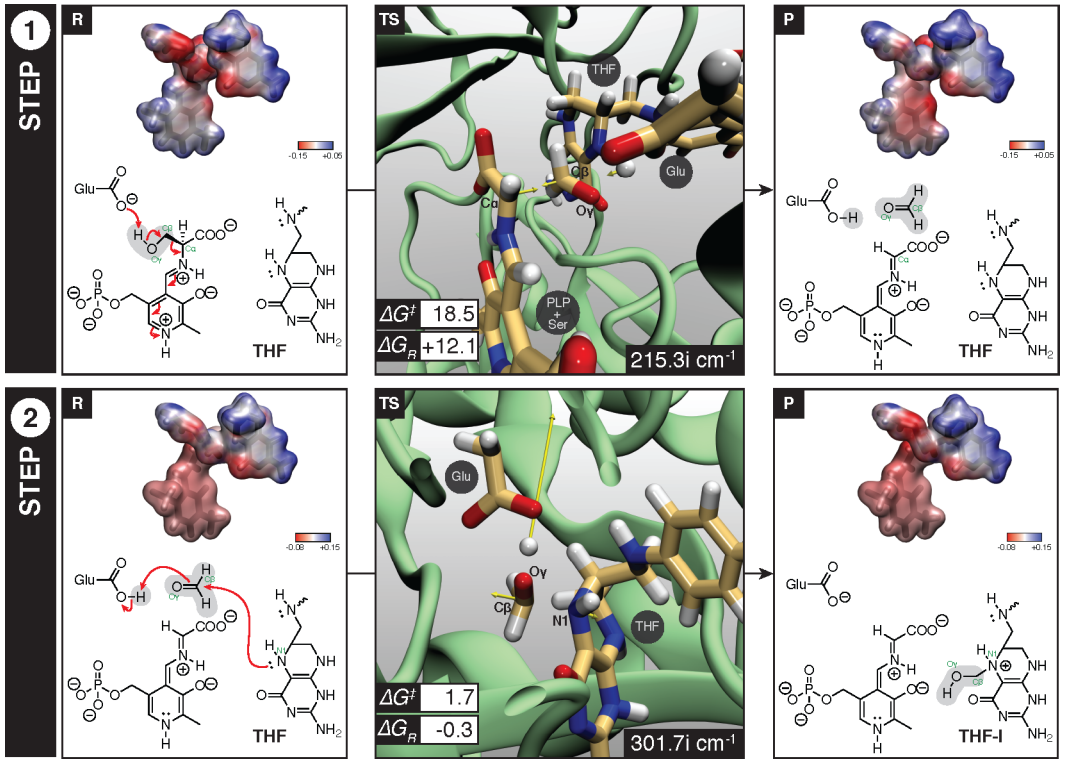

Figure 5. Structures of reactant (R), transition state (TS), and product (P) of the two sequential steps associated with the α-elimination reaction catalyzed by SHMT. Wedge−dash representation of the structures of reactant and product. Three-dimensional representation of the TS structure. The yellow arrows correspond to the major vibrational frequency associated with the imaginary frequency of the TS. The electrostatic potential was calculated and mapped on the surface of the molecules involved in the reaction.

3.1. First Stage: The α-Elimination. The α-elimination of the hydroxymethyl group of the L-Ser is the main point of discussion, with regard to the catalytic mechanism of the SHMT. In the literature, there are two proposals for this reaction. In the first one, it is proposed that Glu57 is protonated and involves the nucleophilic attack of nitrogen N1 from THF to carbon Cβ of the substrate, and from this results the elimination of the hydroxymethyl group.[15−17] (See the top portion of Figure 4.)

The other hypothesis proposes that the Glu57 residue is not protonated and, at the beginning of the reaction, it abstracts a proton from the hydroxyl group of the substrate. From this reaction results the formation of formaldehyde that, afterward,

DOI: 10.1021/acscatal.8b02321
ACS Catal. 2018, 8, 10096−10110

reacts with the nitrogen N1 from THF and becomes covalently bonded to it. (See the bottom portion of Figure 4.)

3.1.1. Unprotonated Glu57. When Glu57 is not protonated, it interacts with the hydroxyl group of the external aldimine by a hydrogen bond, and this interaction endorses a good alignment of the latter group with the THF cofactor. This interaction will be very important during the two steps that are required for the α-elimination process.

The first step is characterized by a proton transfer between the hydroxyl group of the external aldimine and the negatively charged Glu57. The computational calculations also show that this reaction triggers, simultaneously, the cleavage of the bond between carbons Cα and Cβ (the α-elimination reaction) and the formation of a double bond between oxygen Oγ and carbon Cβ (R: 1.38 Å to P: 1.23 Å). At the end of this reaction, one molecule of formaldehyde is obtained, Glu57 becomes protonated, and the PLP cofactor adopts a quinonoid configuration that is negatively charged (Charge of PLP's ring: R: +0.18 au; P: −0.04 au) (see Figure 5, Step 1). This reaction requires an activation Gibbs energy of 18.0 kcal/mol, and it is endergonic in 8.1 kcal/mol.

The TS structure of this reaction is characterized by one imaginary frequency at 229.1i cm^{-1} that is associated with the vibration of the atoms involved in the reaction (see Figure 5, Step 1, center). In the TS structure, the bond that is cleaved is perpendicular to the PLP cofactor ring (Cβ-Cα−C7-C2 angle = 98.6°), a condition that is important in the chemistry of the PLP cofactor to have the reaction kinetically favored.[58,59]

The second step involves the nucleophilic attack of nitrogen N1 of THF to carbon Cβ of the recently formed formaldehyde, and the simultaneous proton transfer from Glu57 to oxygen Oγ of formaldehyde. At the end of this reaction, a hydroxymethyl group is obtained that becomes covalently bonded to the THF cofactor, which becomes positively charged (reactant (R): −1.74; product (P): −1.17). In this step, the quinonoid intermediate that resulted from the first step does not participate in the reaction. (See Figure 5, Step 2.)

The TS of this reaction is characterized by one imaginary frequency at 206.8i cm^{-1}, in which carbon Cβ of formaldehyde adopts an sp3 hybridization and the bond between carbon Cβ and oxygen Oγ becomes elongated, preparing it for the nucleophilic attack endorsed by the THF and the proton transfer from Glu57, respectively.

This reaction requires a very low Gibbs activation energy (2.0 kcal/mol), and it is thermoneutral.

3.1.2. Protonated Glu57. When Glu57 is protonated, the α-elimination occurs in a single step. However, the computational results show that the nucleophilic attack of nitrogen N1 from THF to carbon Cβ of the external aldimine is impossible under biological conditions, since the activation barrier is too high ($\Delta E^{\ddagger}$ = 53.9 kcal/mol) to occur under reasonable conditions of temperature and pressure. In addition, the reaction is very endothermic (ΔE_R = 46.7 kcal/mol) which results from the lack of stabilization endorsed by Glu57, contrasting to what was observed with the previous model. Therefore, these results indicate that Glu57 cannot be protonated during the α-elimination of the external aldimine by the SHMT. (See Figure 6.)

3.2. Second Stage: Conversion of THF Intermediate to 5,10-Methylene−THF. After the α-elimination stage, the THF is covalently bonded to a hydroxymethyl group and becomes positively charged. The next step involves the cyclization of this reaction intermediate (THF-I) to yield one of the final products of the reaction: the 5,10-methylene−THF.

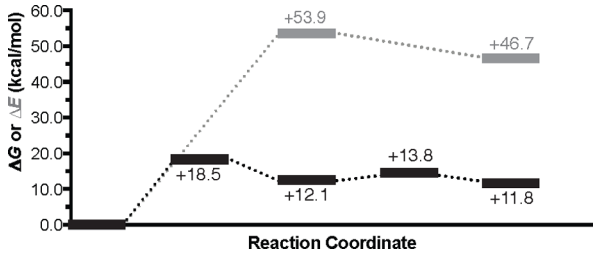

Figure 6. Energy profile of the two evaluated mechanisms for the α-elimination process catalyzed by SHMT with Glu57 protonated (ΔE) (gray) or unprotonated (ΔG) (black).

In the literature, there are two hypotheses for this reaction. Some authors propose that this reaction does not require participation of the enzyme, and therefore, it could occur in the cytoplasm of the cell (water environment). Other authors suggest that the reaction must continue inside of the enzyme since the cyclization process is a rather complex task and the enzyme will be very important to catalyze this process.[15,19] Each of these two hypotheses is discussed below.

3.2.1. Enzymatic Catalysis. Under enzymatic catalysis, the formation of 5,10-methylene−THF requires five steps, which include (i) three proton transfers, (ii) the formation and release of one water molecule, and (iii) the cyclization process. In most of these reactions, Glu57 plays an active role, and it is directly involved in the catalysis. The quinonoid intermediate (PLP cofactor) is neither involved in any of these reactions nor does it affect the cyclization process. However, it was kept in all of the models used to study these reactions, because it remains in the quinonoid intermediate stage, waiting for the final reaction, where it is protonated.

*3.2.1.1. **Proton Transfer Reactions**.* The first two steps consist of three proton transfers. The first step involves the intramolecular proton transfer from nitrogen N1 to nitrogen N4, resulting in the migration of the positive charge that was concentrated at nitrogen N1, in the reactant, to nitrogen N4. This reaction has a very small Gibbs activation energy ($\Delta G^{\ddagger}$ = 0.7 kcal/mol), and it is exergonic in 8.5 kcal/mol.

The low activation energy results from the configuration of the TS structure (1230.6i cm^{-1}), in which both N atoms are very close to each other, favoring the proton transfer (N1−N4 = 2.69 Å). The proximity between both atoms is endorsed by Gly57 that establishes two hydrogen bonds with the THF intermediate: one with the hydroxyl group (1.47 Å) and another with the proton that is bonded to nitrogen N4 (2.57 Å). The stabilization of the product of the reaction relies on the better delocalization of the positive charge (mesomeric effect) that is provided by the benzyl group that is attached to nitrogen N4. (See Figure 7, Step 3.)

The second step involves two coupled proton transfers: one between nitrogen N4 to oxygen Oγ and another between oxygen Oγ and Glu57. The full process is almost spontaneous ($\Delta G^{\ddagger}$ = 1.3 kcal/mol), and the reaction is very exergonic in 8.3 kcal/mol (see Figure 7, Step 4). The low activation energy of this reaction is only possible because of the proximity of the atoms involved in the chemical reaction at the TS structure (639.6i cm^{-1}). The higher stabilization of the product (THF-III) of this reaction is due to the absence of point charges in the active site, which contrasts with the reactants where

DOI: 10.1021/acscatal.8b02321
ACS Catal. 2018, 8, 10096−10110

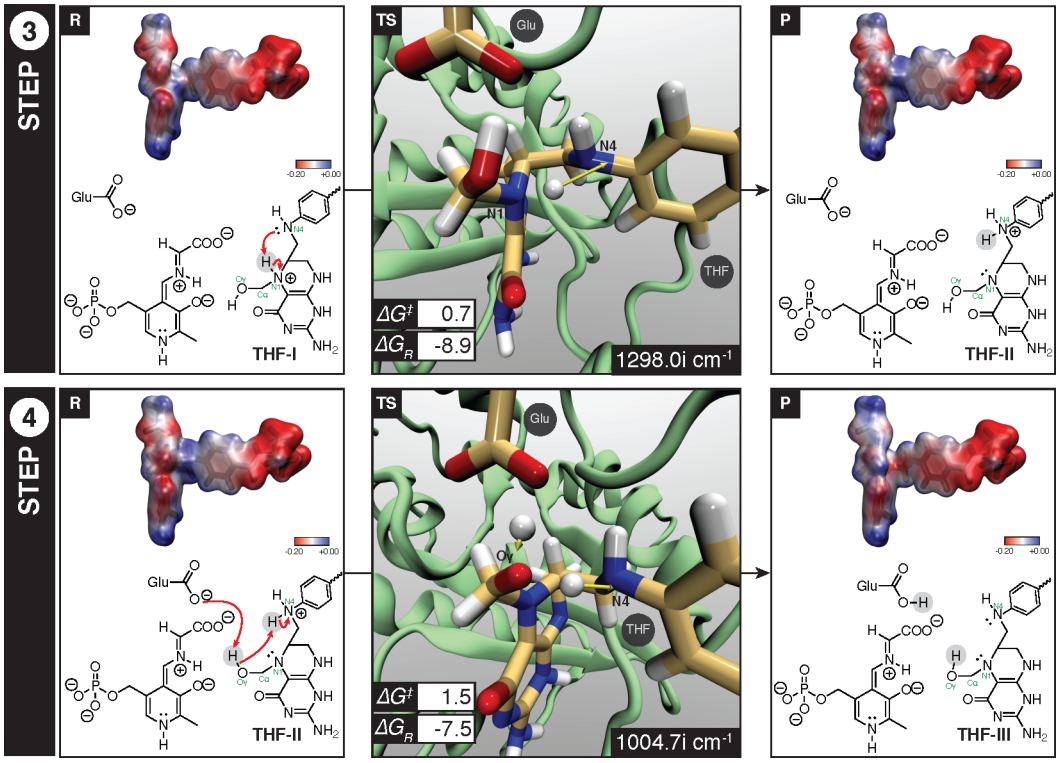

Figure 7. Structures of reactant (R), transition state (TS), and product (P) of the two sequential steps associated with the three proton transfers catalyzed by SHMT. Wedge−dash representation of the structures of reactant and product. Three-dimensional representation of the TS structure. The yellow arrows correspond to the major vibrational frequency associated with the imaginary frequency of the TS. The electrostatic potential was calculated and mapped on the surface of the molecules involved in the reaction.

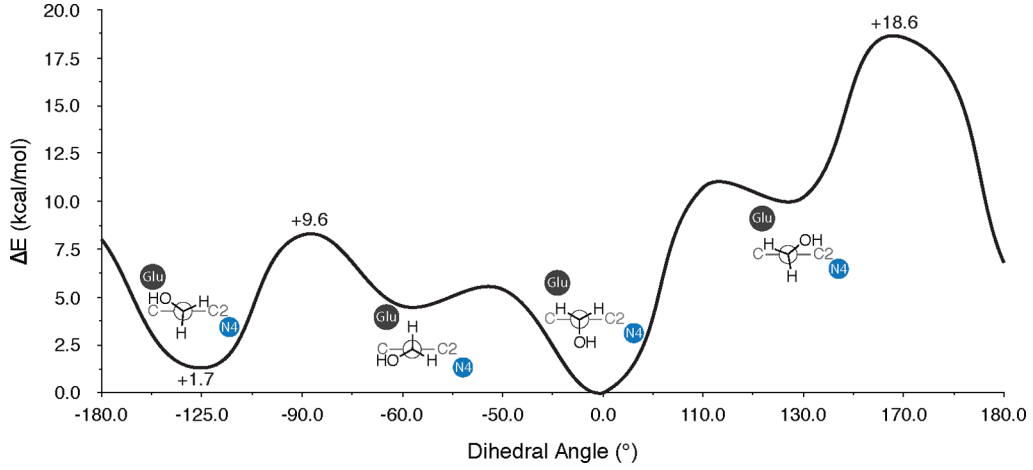

Figure 8. Energy profile for the dihedral rotation across the N1−Cβ bond. Newman representation was used to show the relative configuration of the Cβ and N1 atoms. The energies were computed using the ONIOM(DLPNO−CCSD(T)/CBS:ff99SB) scheme. The full energy profile obtained from the scan for rotational increments of 5.0° can be found in Figure S2 in the SI.

nitrogen N4 of the THF intermediate (THF-II) was positively charged, and Glu57 was negatively charged. This effect can be seen in the electrostatic maps represented in Figure 7. The key role played by Glu57 in these two steps reinforces, once again, its importance in the catalytic process, as well as the importance of its protonation state at the beginning of the catalytic process.

3.2.1.2. ***Dehydration Reaction.*** The next step of the cyclization process involves the formation of a carbocation through the elimination of a water molecule.

Our initial attempts to study this reaction involved the direct protonation of the hydroxyl group by Glu57 that led to the formation of a water molecule, which should dissociate subsequently (Figure 7, Step 4).

Although this step is rather straightforward, the computational results indicate that this reaction is only possible when the hydroxyl group does not interact with nitrogen N4 by a hydrogen bond. Only in this conformation, it was possible to characterize a TS structure for the dehydration process. This new conformation is possible through the rotation of the N1−

DOI: 10.1021/acscatal.8b02321
ACS Catal. 2018, 8, 10096−10110

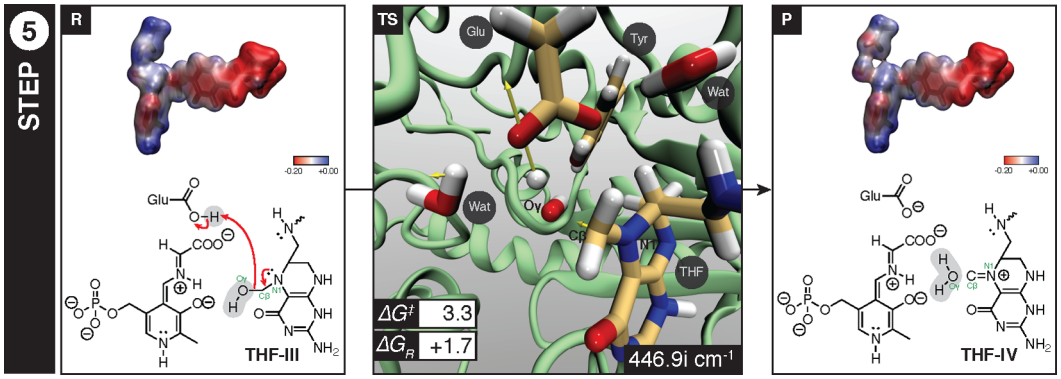

Figure 9. Structures of reactant (R), transition state (TS), and product (P) of the dehydration of the THF intermediate catalyzed by the SHMT. Wedge−dash representation of the structures of reactant and product. Three-dimensional representation of the TS structure. The yellow arrows correspond to the major vibrational frequency associated with the imaginary frequency of the TS. The electrostatic potential was calculated and mapped at the surface of the molecules involved in the reaction.

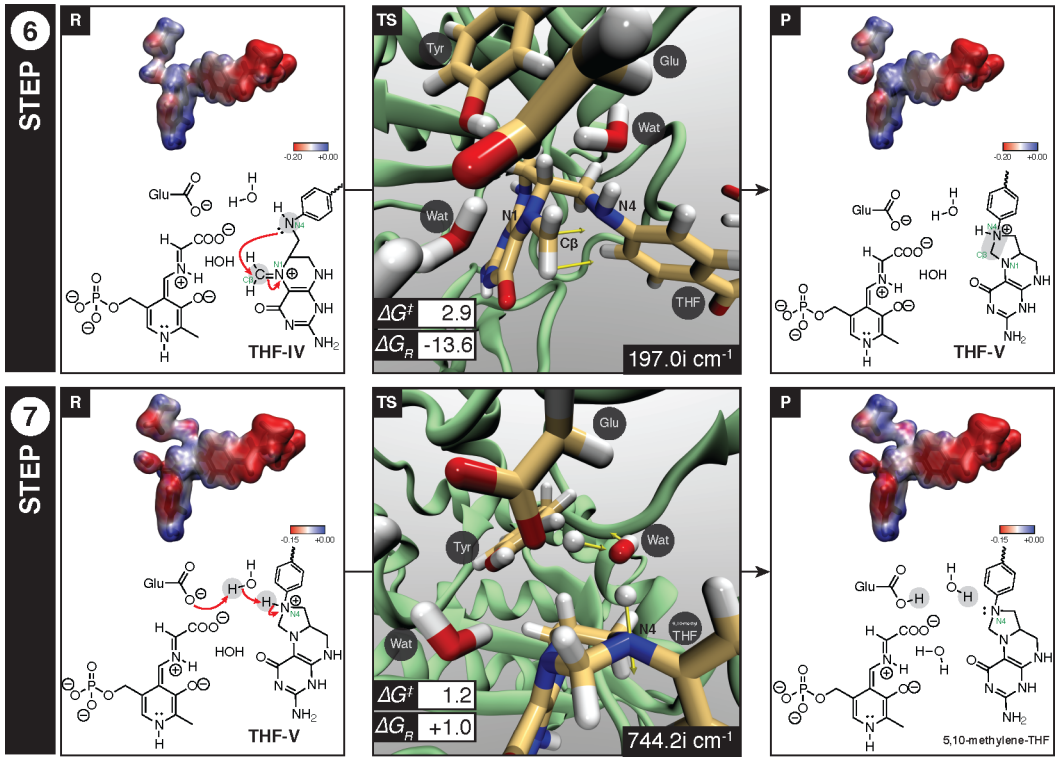

Figure 10. Structures of reactant (R), transition state (TS), and product (P) of the steps involved in cyclization of the THF intermediate catalyzed by the SHMT. Wedge−dash representation of the structures of reactant and product. Three-dimensional representation of the TS structure. The yellow arrows corresponds to the major vibrational frequency associated with the imaginary frequency of the TS. The electrostatic potential was calculated and mapped on the surface of the molecules involved in the reaction.

Cβ bond from the product of the previous step by −125.0° and requires an energy cost of 9.6 kcal/mol (see Figure 8).

In the new conformation of the THF intermediate (THF-III), the elimination of the water molecule requires a Gibbs activation energy of 5.4 kcal/mol, and the reaction is slightly endergonic in 3.0 kcal/mol.

The small activation energy of this reaction results from the good alignment between Glu57 and the hydroxyl group of the THF intermediate in the TS structure (113.6i cm^{-1}) (see Figure 9). Although, in this new conformation, Glu57 does not interact directly with nitrogen N4, it establishes a hydrogen bond with a water molecule (1.83 Å) that interacts with nitrogen N4 by another hydrogen bond (2.00 Å).

At the end of this step, the release of the water molecule restores the negative charge of Glu57 and generates a positive charge at nitrogen N1 that becomes bonded to carbon Cβ by a double bond (N1−Cβ R: 1.43 Å to P: 1.32 Å). The formation of the new point charges in the THF intermediate (THF-IV) are very important, since they polarize the Cβ-N1 bond that will be crucial to increase the electrophilic character of the Cβ atom, which is required for the cyclization of the THF intermediate (THF-IV) in the next step.

3.2.1.3. ***Cyclization.*** The cyclization of the THF intermediate (THF-IV) to yield the 5,10-methylene−THF molecule requires two sequential steps: (i) an intramolecular nucleophilic attack and (ii) a deprotonation.

DOI: 10.1021/acscatal.8b02321
ACS Catal. 2018, 8, 10096−10110

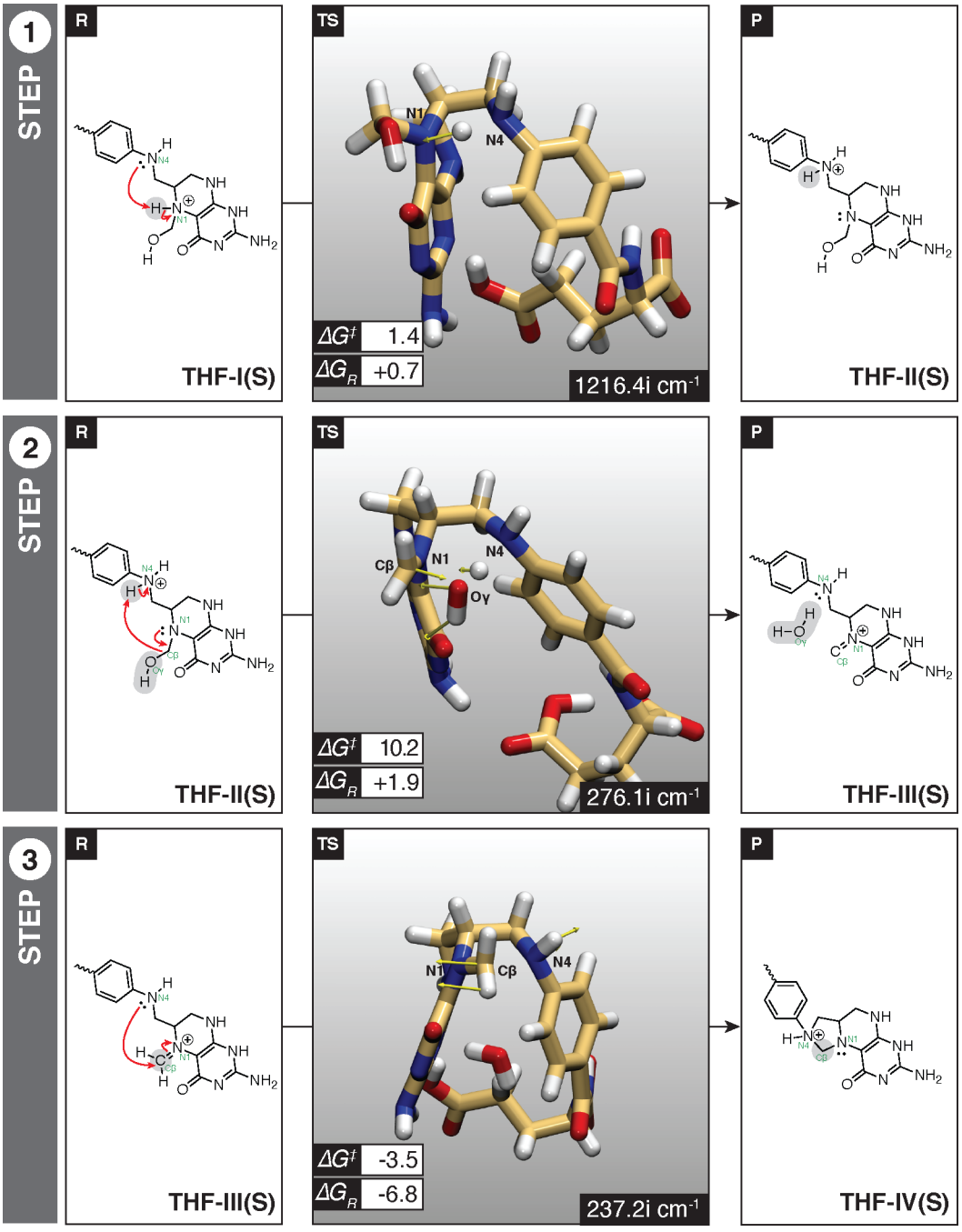

Figure 11. Structures of reactant (R), transition state (TS), and product (P) of the steps involved in cyclization of the THF intermediate in the cytoplasm. Wedge−dash representation of the structures of reactant and product. Three-dimensional representation of the TS structure. The yellow arrows correspond to the major vibrational frequency associated with the imaginary frequency of the TS.

The first step involves the nucleophilic attack of nitrogen N4 to carbon Cβ of the THF intermediate (THF-IV), from which results a 5-membered ring. This reaction is favored by the correct orientation of carbon Cβ, in relation to nitrogen N4, which is endorsed by the hydrogen bond that Glu57 establishes with one water molecule present in the active site and the latter one with nitrogen N4. For this reason, the TS structure (205.0i cm^{-1}) is very close to the reactant of this reaction, from which results a spontaneous reaction (see Figure 10, Step 6). The positive charge that was lodged at nitrogen N1 of the THF intermediate (THF-IV) migrates at the end of the reaction to nitrogen N4, where it is better delocalized due to the presence of the neighbor benzyl group that is bonded to the nitrogen N4. The Gibbs reaction energy of this reaction reflects this stabilization being exergonic in 16.9 kcal/mol.

The next step of the cyclization process involves the proton transfer from nitrogen N4 of the THF intermediate (THF-V) to Glu57. This reaction proceeds with the participation of a water molecule that catalyzes the proton transfer between both groups. The TS of this reaction is characterized by one imaginary frequency at 670.7i cm^{-1}. At the end of the reaction, Glu57 becomes protonated and one of the final products of the enzymatic catalysis, 5,10-methylene−THF, is obtained.

DOI: 10.1021/acscatal.8b02321
ACS Catal. 2018, 8, 10096−10110

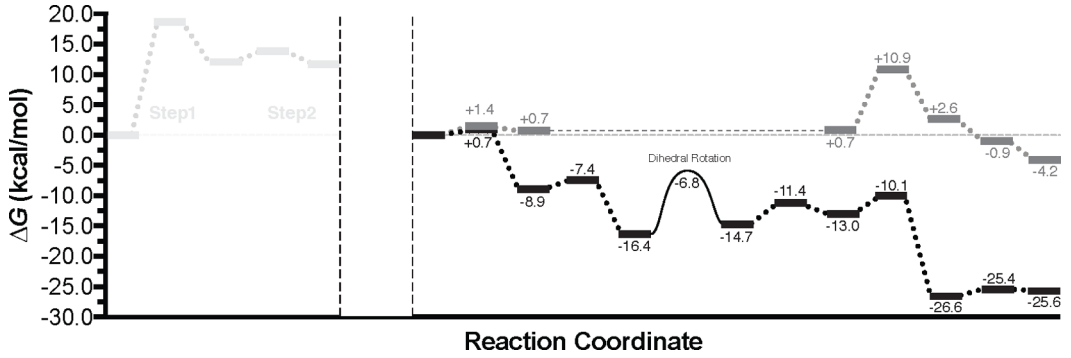

Figure 12. Energy profile of the two proposals for the conversion of the THF intermediate into 5,10-methylene−THF: black color indicates that the process is catalyzed by the SHMT enzyme, and gray color indicates that the reactions occur in the cytoplasm. The values in brackets correspond to the energy of each single step.

This step is almost spontaneous, requiring a Gibbs activation energy of 1.1 kcal/mol, and the reaction is slightly endergonic in 0.5 kcal/mol (see Figure 10, Step 7).

Overall, it can be concluded that the cyclization process requires a Gibbs activation energy of 1.1 kcal/mol and it is exergonic in 16.4 kcal/mol.

3.2.2. Nonenzymatic Catalysis. The last section described the synthesis of the 5,10-methylene−THF molecule under enzymatic catalysis. This section describes the energy profile of the same reaction that resembles the cytoplasm, and it is modeled as a water environment.

Under enzymatic catalysis, the full process requires five sequential steps, in which Glu57 plays an active role involving a conformational rearrangement (the rotation of the N1−Cβ bond) of the THF intermediate (THF-I(S)). In the cytoplasm, the cyclization process requires only three steps and does not require any conformational rearrangement of THF.

The first step of the reaction in the cytoplasm is very similar to that which occurs during the enzyme catalysis (see Figure 11, Step 1, and Figure 7, Step 3). It involves the proton transfer from nitrogen N1 to nitrogen N4 of the THF reaction intermediate (THF-I(S) versus THF-I).

In the cytoplasm, the reaction is marginally slower, requiring a Gibbs activation energy of 1.4 kcal/mol (versus 0.7 kcal/mol in the enzymatic catalysis). The most significant difference is observed in the free energy of the reaction. In the cytoplasm, this step is endergonic in 0.7 kcal/mol, whereas, under enzymatic catalysis, it is exergonic in 8.5 kcal/mol. This difference comes from the stabilization of the product of the reaction that is provided by the enzyme, and mainly by Glu57, which, in the cytoplasm, is absent.

The next step involves the dehydration process. This is where the differences between both mechanisms are observed. In the cytoplasm, the abstraction of the proton bonded to nitrogen N4 by oxygen Oγ occurs in a single step without requiring any conformational rearrangement of the reaction intermediate. At the end of this step, one water molecule is formed, and the same reactional product is obtained. Despite the simplicity of the reaction, the energetic cost for this reaction in the cytoplasm is much higher than under enzymatic catalysis. In the cytoplasm, this step requires a Gibbs activation energy of 10.2 kcal/mol (versus 5.4 kcal/mol), which means that the dehydration process is ∼3000 times slower than when it happens with enzymatic catalysis. As expected, the Gibbs free energy of reaction is almost the same for the dehydration, whether the reaction occurs under enzymatic catalysis (ΔG_R = +3.0 kcal/mol) or in the cytoplasm (ΔG_R = +1.9 kcal/mol) (see Figure 11, Step 2, and Figure 9, Step 5).

The last step required for the cyclization of the THF intermediate (THF-III(S) versus THF-IV) involves the nucleophilic attack of nitrogen N4 to carbon Cβ. This reaction is spontaneous in both the cytoplasm and the enzyme ($\Delta G^{\ddagger}$ = −3.5 kcal/mol versus $\Delta G^{\ddagger}$ = −1.4 kcal/mol), which means that both processes are energetically similar (see Figure 11, Step 3, and Figure 10, Step 6). However, it requires only one step, instead of two. This energy difference is explained by the greater freedom of the structure in the cytoplasm, which allows an easier cyclization of the 5-membered ring of THF without the geometric constraints imposed by the active site of the enzyme. However, once more, the enzyme is able to provide further stabilization of the reactional product (ΔG_R = −16.9 kcal/mol versus ΔG_R = −6.8 kcal/mol), contributing to a more favorable reaction.

All the TS structure of these reactions were checked using the vibrational frequency analysis and are characterized by a single imaginary frequency for each TS. Those frequencies correspond to the vibration of the atoms directly involved in each step and can be found in Figure 11.

Looking at the overall results for the cyclization of the THF intermediate in the cytoplasm, it can be concluded that, although the reaction in the water requires fewer steps (three instead of four steps), the reaction, from the kinetic and thermodynamic point of view, is favored with enzymatic catalysis. Under enzymatic catalysis, the rate-limiting step of the cyclization process is the dihedral rotation across the N1−Cβ bond and requires 9.6 kcal/mol, whereas, in the cytoplasm, the rate-limiting step is the elimination of the water molecule with an activation barrier of 10.2 kcal/mol (see Figure 12). When the reaction occurs in water, the process is almost thermoneutral (−4.2 kcal/mol), whereas with enzymatic catalysis of the same process originates a product that is highly stabilized in 28.5 kcal/mol (see Figure 12).

In sum, these results show that the production of the 5,10-methylene−THF can occur in the cytoplasm and without enzymatic catalysis, but it would be much slower. However, taking into account that this process requires the migration of the THF intermediate to the cytoplasm, which implies an additional energetic cost (dissociation and desolvation effects), the full process will be even slower. For this reason, the cyclization of THF intermediate (THF-I) has to occur through an enzymatic process catalyzed by the SHMT.

DOI: 10.1021/acscatal.8b02321
ACS Catal. 2018, 8, 10096−10110

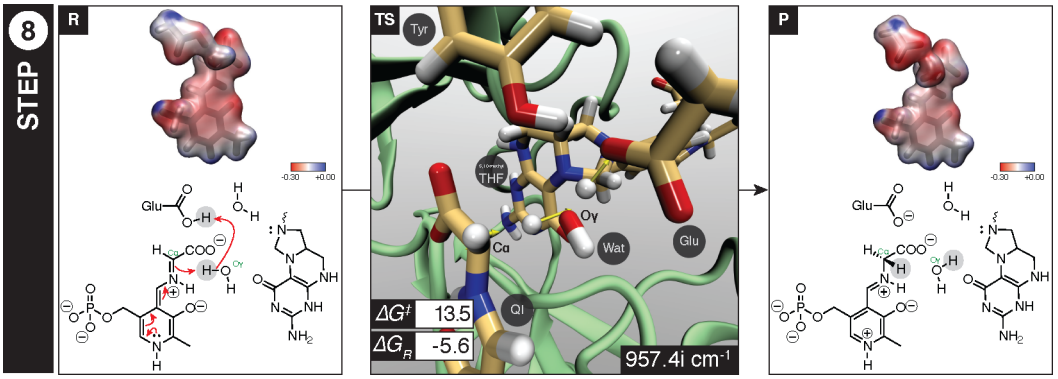

Figure 13. Structures of reactant (R), transition state (TS), and product (P) of the protonation of the quinonoid intermediate (QI) catalyzed by the SHMT. Wedge−dash representation of the structures of reactant and product. Three-dimensional representation of the TS structure. The yellow arrows correspond to the major vibrational frequencies associated with the imaginary frequency of the TS. The electrostatic potential was calculated and mapped on the surface of the molecules involved in the reaction.

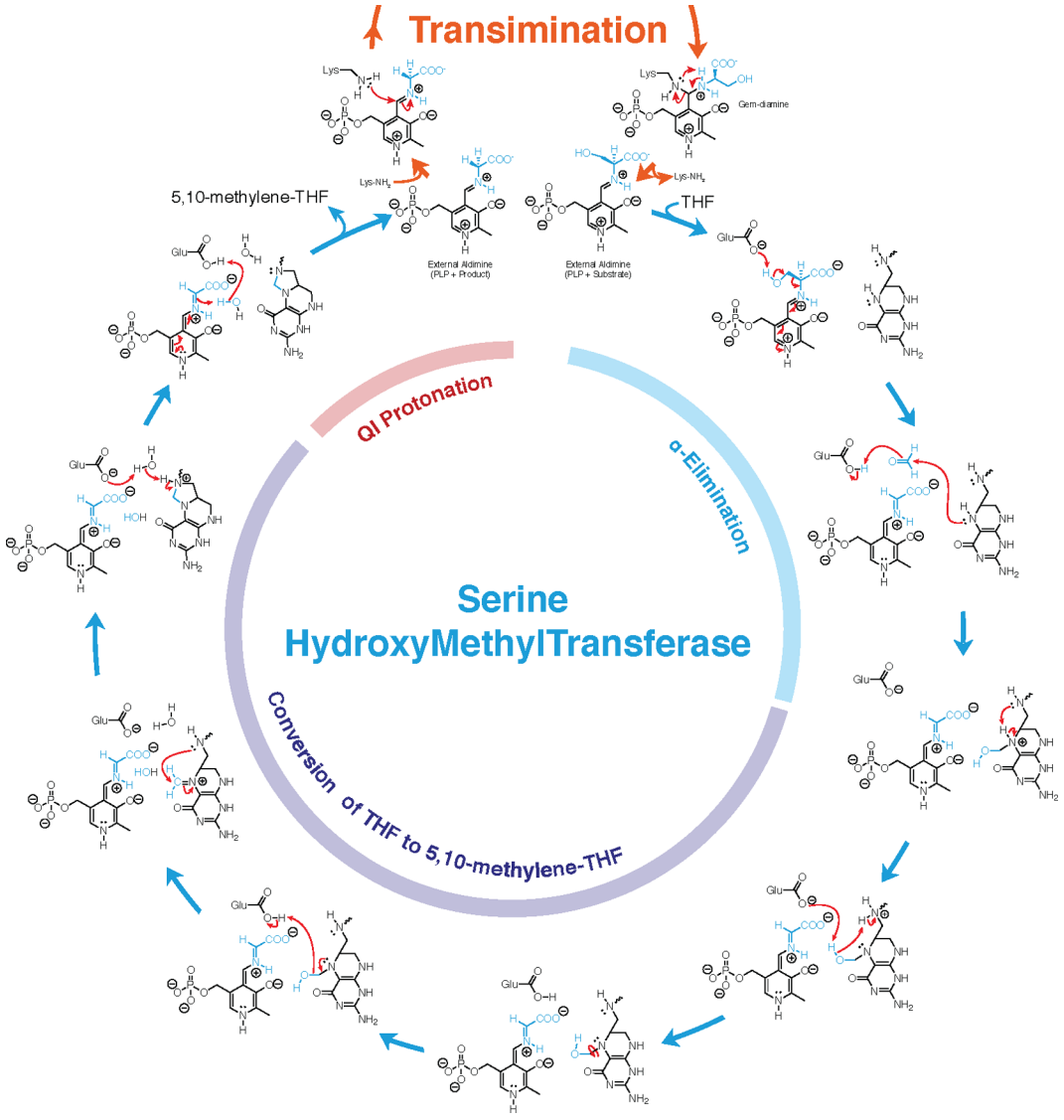

Figure 14. Overview of the catalytic mechanism of the PLP-dependent enzyme SHMT obtained in this work.

3.3. Protonation of the Quinonoid Intermediate. Once the 5,10-methylene−THF is formed, the active site has protonated Glu57 and a quinonoid intermediate (Figure 10, Step 7) that must be converted to an internal aldimine in order to enhance the enzymatic turnover and the release of one molecule of Gly.

Note that whether the 5,10-methylene−THF is released from the SHMT active site to the cytoplasm before or after the

DOI: 10.1021/acscatal.8b02321
ACS Catal. 2018, 8, 10096−10110

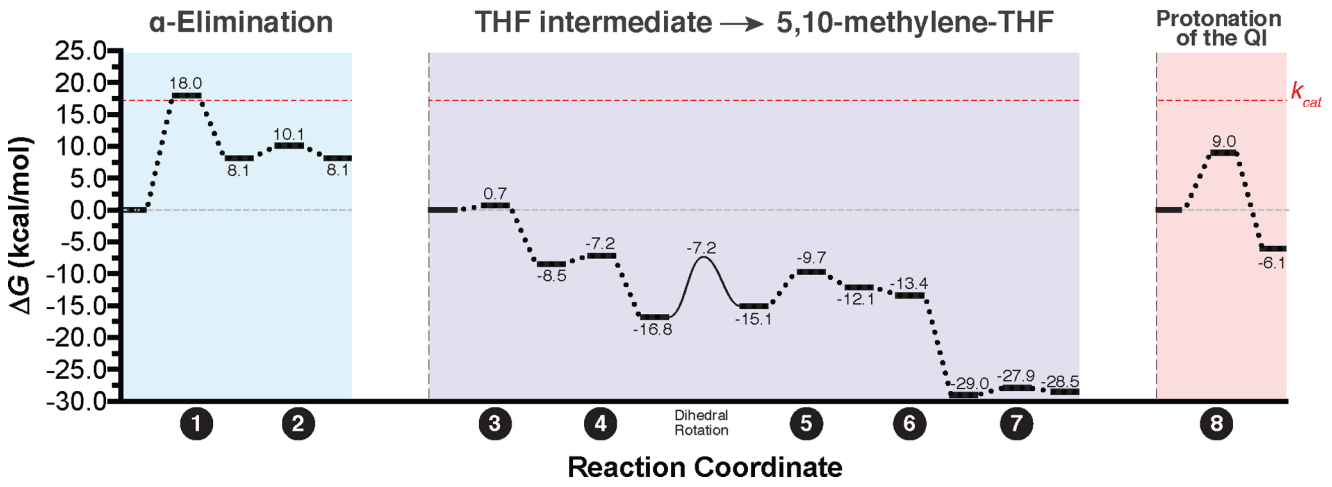

Figure 15. Complete energy profile (DLPNO−CCSD(T)/CBS::ff99SB) for the catalysis of L-serine and THF into glycine and 5,10-methylene−THF by the SHMT.

protonation of the quinonoid intermediate is unknown. For this reason, we chose to maintain the 5,10-methylene−THF inside the active site during this step. We observed that it is neither involved in any chemical step nor is it involved in the catalytic process.

This step involves a proton transfer from Glu57 to carbon Cα of the QI, through a water molecule that catalyzes the reaction. This water molecule is the one that was generated at Step 5 in Figure 9, which, in this final step, plays an important role in the continuity of the catalytic process. This reaction has a Gibbs activation energy of 9.0 kcal/mol, and it is exergonic in 6.1 kcal/mol. The TS was validated through the vibrational frequencies analysis, showing a single imaginary frequency assigned to the atoms that are intrinsically related to the reaction (775.0i cm^{-1}). This reaction is favored because the QI is negatively charged and, therefore, it meets good conditions to act as a nucleophile and becomes protonated (see Figure 13).

At the end of this reaction, Glu57 becomes negatively charged, restoring its initial protonation state, and an external aldimine with a Gly bonded to the PLP cofactor is obtained. After the transimination reaction—which is a process that is common to all PLP-dependent enzymes—Gly is released from the active site, and the PLP cofactor becomes bonded to the active site Lys229, forming an internal aldimine, which makes the enzyme ready for a new catalytic cycle, once the substrate becomes available.

4. CONCLUSION

In this work, the catalytic mechanism of the SHMT was studied by computational means that employ QM/MM methodologies. This enzyme catalyzes the reversible conversion of L-serine and THF to glycine and 5,10-methylene−THF, with the help of the PLP cofactor. The reaction requires eight sequential steps that can be divided into three main stages: the α-elimination, the cyclization of the 5-hydroxymethyl−THF intermediate into 5,10-methylene−THF, and the protonation of the quinonoid intermediate (QI).

The full mechanism is represented in Figure 14. In the first step, the hydroxymethyl group of the substrate is eliminated in the form of a formaldehyde molecule that, in the second step, undergoes a nucleophilic attack by the nitrogen N1 of the THF cofactor. The resulting THF intermediate (THF-I) undergoes an intramolecular reaction that involves a proton transfer from the nitrogen N1 to nitrogen N4 (Step 3) and finally to Glu57 (Step 4). Afterward, a conformational rearrangement of the THF intermediate (THF-III) occurs, which is required for the elimination of a water molecule that enhances the electrophilic nature of carbon Cβ, which, in turn, is required for the next step (Step 5). Subsequently, carbon Cβ becomes suitable to undergo a nucleophilic attack by nitrogen N4, producing a 5-membered ring THF intermediate (Step 6). Immediately after, Glu57 abstracts the remaining proton from the nitrogen N4 and originates the final product 5,10-methylene−THF (Step 7). Finally, the water molecule that was released in Step 5 assists, in the final step, the proton transfer from the Glu57 to the carbon Cα of the QI producing an external aldimine with the glycine bonded to the PLP cofactor (Step 8). At the end of this reaction, the release of 5,10-methylene−THF and L-Gly (after the transimination reaction) from the active site occurs, and the enzyme is ready for a new enzymatic cycle.

According to the calculated energy profile (Figure 15), the rate-limiting step of the entire mechanism is where the elimination of the hydroxymethyl group occurs, forming a formaldehyde intermediate that becomes immediately bonded to the THF cofactor. The α-elimination reaction requires an activation energy boost of 18.0 kcal/mol. These results closely fit the experimental kinetic data that predicted an activation barrier of 15.7−16.2 kcal/mol.[13,14,60]

Note that SHMT is also capable of catalyzing the reverse reaction, in other words, the conversion of glycine and 5,10-methylene−THF into L-serine and THF. Analyzing the energy profile in the reverse order (Figure 15), all the steps are feasible under biological conditions, agreeing with the experimental evidence of reversible catalysis. However, there is no kinetic result regarding the kinetics of the reverse reaction catalyzed by the SHMT from *E. coli*. There is only a kinetic study using *Hydrogenobacter thermophilus* from which it was concluded that the reaction is almost 4 times slower in the reverse direction.[61] Based on this evidence, a slower conversion of glycine to L-serine might be expected. This also agrees very well with the mechanism proposed in this work, since the rate-limiting step, for the reverse reaction, would be 29.7 kcal/mol, which, compared with the rate-limiting step of the direct catalytic step, would lead to a slower reaction.

DOI: 10.1021/acscatal.8b02321
ACS Catal. 2018, 8, 10096−10110

The results obtained with this work also provide new insights into the catalytic process and on the α-elimination and the production of the 5,10-methylene−THF molecule.

Regarding the two proposals that are available in the literature for the α-elimination reaction, the results presented in this paper indicate that the reaction proceeds with the formation of the formaldehyde molecule as an intermediate, and, only then, it becomes covalently bonded to nitrogen N1 of the THF cofactor. In this process, Glu57 cannot be protonated, since it plays a key role in holding the proton of the hydroxymethyl group (see Figure 15). Although structural studies showed a close proximity between Glu57 and the hydroxyl group of the substrate, from which was suggested that the Glu57 was protonated,[16,17], the calculations showed that this configuration of the active site does not allow the α-elimination. Such reaction was only possible to model when we considered the Glu57 in an anionic form at the beginning of the reaction. When Glu57 is anionic, the hydroxyl group from the substrate establishes a hydrogen bond with the Glu57, according to the experimental evidence that shows a close proximity between the Glu57 residue and the Oγ atom of the substrate.

Glu57 was found to play a key role in several reactions of the mechanism, namely, Steps 1, 2, 4, 5, 7, and 8. This is consistent with the mutagenic studies that show that any mutations to Glu57 caused a drastic inhibition of the enzyme.[16,18] This is the first time where the role played by this residue is explained. Furthermore, Glu57 is a key residue to handle most of the proton transfers that are required for the reaction to occur, holding a negative charge during some steps (steps 3 and 6) to provide conditions for intermediate reactions to happen. Then, Glu57 becomes protonated during the remaining steps of the mechanism. In summary, Glu57 works as an proton pump that handles the charge transfers across the mechanism and establishes a link between the external aldimine and the THF cofactor. (See Figure 16.)

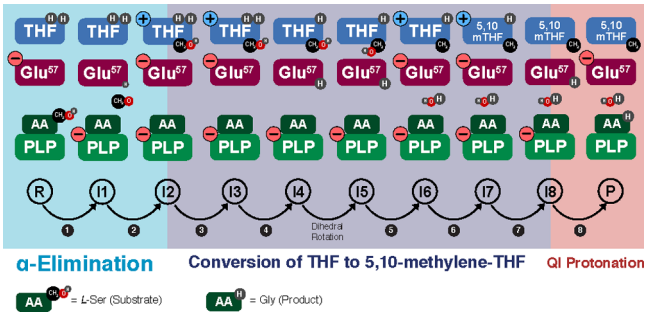

Figure 16. Schematic representation of the behavior of the main groups and charges across the entire catalytic mechanism.

In the literature, there are also two different proposals suggesting that the conversion of the THF intermediate to 5,10-methylene−THF can alternatively occur outside the enzyme through a nonenzymatic mechanism (in the solvent).[15,19] In this work, both proposals were studied, and the results showed that the reaction is thermodynamically and kinetically favored under enzymatic catalysis. The results presented in the manuscript are also consistent with the experimental evidence observed,[15] confirming that the conversion of the THF to 5,10-methylene−THF is very fast and almost spontaneous. Overall, this stage of the mechanism (Step 3 to Step 7) is very exergonic and has low free activation energies, agreeing with the experimental observation of an almost-spontaneous process. In addition, the steps involved in the cyclization of the THF are important to prepare the enzyme for the final step where a proton is transferred to the QI to produce the glycine. This evidence agrees with the fact that the THF cyclization must occur inside the active site of the SHMT.

Moreover, our results agree with the proposal of Dunathan,[59,62] which postulates that the bound complex that is formed or cleaved during the reaction involving the PLP cofactor must be placed perpendicular to the conjugated system of the PLP. The hydroxymethyl group is released almost perpendicular to the PLP cofactor (Cβ-Cα−C7-C2 angle = 98.6°), and the protonation of the QI occurs in the same way (H−Cα−C7-C2 angle = 115.7°).

Together with the previous stages that are common to all PLP-dependent enzymes, this work provides, for the first time, and with an atomistic level of detail, a portrait of the entire mechanism catalyzed by the SHMT. We believe that this knowledge provides valuable information for the rational molecular design of new drugs against malaria.

■ ASSOCIATED CONTENT

Supporting Information

The Supporting Information is available free of charge on the ACS Publications website at DOI: 10.1021/acscatal.8b02321.

Alignment of the protein sequences of the *E. coli* and *P. falciparum* forms of the SHMT enzyme and tridimensional image of the overlapping of the structures of all dimer or active site residues (Figure S1); energy profile of the dihedral rotation across the N1−Cβ bond of the THF intermediate (Figure S2); analysis of all key interactions for each step of the catalytic mechanism (Figure S3) (PDF)

Molecular mechanics parameters for the external aldimine (PLP + glycine) and 5-hydroxymethyl−THF (ZIP)

PDB coordinate files for all stationary states of the entire catalytic mechanism of SHMT (ZIP)

■ AUTHOR INFORMATION

Corresponding Author

*E-mail: nscerque@fc.up.pt.

ORCID

Henrique S. Fernandes: 0000-0002-9280-1838

Maria João Ramos: 0000-0002-7554-8324

Present Address

§UCIBIO@REQUIMTE, BioSIM, Departamento de Biomedicina, Faculdade de Medicina da Universidade do Porto, Alameda Professor Hernâni Monteiro, 4200−319, Porto, Portugal.

Notes

The authors declare no competing financial interest.

■ ACKNOWLEDGMENTS

European Union (FEDER funds POCI/01/0145/FEDER/007728) and National Funds (FCT/MEC, Fundação para a Ciência e Tecnologia and Ministério da Educação e Ciência) under the Partnership Agreement PT2020 UID/MULTI/04378/2013.UID/MULTI/04378/2013; NORTE-01-0145-

DOI: 10.1021/acscatal.8b02321
ACS Catal. 2018, 8, 10096−10110

FEDER-000024, supported by Norte Portugal Regional Operational Programme (NORTE 2020), under the PORTUGAL 2020 Partnership Agreement, through the European Regional Development Fund (ERDF); Fundação para a Ciência e a Tecnologia (FCT) through Project IF/01310/2013/CP1208/CT0002 and PTDC/QUI-QFI/31689/2017. H.F. is grateful to the Fundação para a Ciência e Tecnologia (FCT), Portugal for a PhD Grant (No. SFRH/BD/115396/2016).

REFERENCES

(1) Haldar, K.; Bhattacharjee, S.; Safeukui, I. Drug resistance in Plasmodium. *Nat. Rev. Microbiol.* **2018**, *16*, 156.

(2) *World Malaria Report 2017*; World Health Organisation: Geneva, Switzerland, 2017.

(3) Baragaña, B.; Hallyburton, I.; Lee, M. C. S.; Norcross, N. R.; Grimaldi, R.; Otto, T. D.; Proto, W. R.; Blagborough, A. M.; Meister, S.; Wirjanata, G.; Ruecker, A.; Upton, L. M.; Abraham, T. S.; Almeida, M. J.; Pradhan, A.; Porzelle, A.; Martínez, M. S.; Bolscher, J. M.; Woodland, A.; Luksch, T.; Norval, S.; Zuccotto, F.; Thomas, J.; Simeons, F.; Stojanovski, L.; Osuna-Cabello, M.; Brock, P. M.; Churcher, T. S.; Sala, K. A.; Zakutansky, S. E.; Jiménez-Díaz, M. B.; Sanz, L. M.; Riley, J.; Basak, R.; Campbell, M.; Avery, V. M.; Sauerwein, R. W.; Dechering, K. J.; Noviyanti, R.; Campo, B.; Frearson, J. A.; Angulo-Barturen, I.; Ferrer-Bazaga, S.; Gamo, F. J.; Wyatt, P. G.; Leroy, D.; Siegl, P.; Delves, M. J.; Kyle, D. E.; Wittlin, S.; Marfurt, J.; Price, R. N.; Sinden, R. E.; Winzeler, E. A.; Charman, S. A.; Bebrevska, L.; Gray, D. W.; Campbell, S.; Fairlamb, A. H.; Willis, P. A.; Rayner, J. C.; Fidock, D. A.; Read, K. D.; Gilbert, I. H. A novel multiple-stage antimalarial agent that inhibits protein synthesis. *Nature* **2015**, *522*, 315.

(4) McCarthy, J. S.; Lotharius, J.; Rückle, T.; Chalon, S.; Phillips, M. A.; Elliott, S.; Sekuloski, S.; Griffin, P.; Ng, C. L.; Fidock, D. A.; Marquart, L.; Williams, N. S.; Gobeau, N.; Bebrevska, L.; Rosario, M.; Marsh, K.; Möhrle, J. J. Safety, tolerability, pharmacokinetics, and activity of the novel long-acting antimalarial DSM265: a two-part first-in-human phase 1a/1b randomised study. *Lancet Infect. Dis.* **2017**, *17*, 626−635.

(5) Kronenberger, T.; Lindner, J.; Meissner, K. A.; Zimbres, F. M.; Coronado, M. A.; Sauer, F. M.; Schettert, I.; Wrenger, C. Vitamin B6-dependent enzymes in the human malaria parasite Plasmodium falciparum: a druggable target? *BioMed Res. Int.* **2014**, *2014*, 108516.

(6) Schwertz, G.; Witschel, M. C.; Rottmann, M.; Bonnert, R.; Leartsakulpanich, U.; Chitnumsub, P.; Jaruwat, A.; Ittarat, W.; Schafer, A.; Aponte, R. A.; Charman, S. A.; White, K. L.; Kundu, A.; Sadhukhan, S.; Lloyd, M.; Freiberg, G. M.; Srikumaran, M.; Siggel, M.; Zwyssig, A.; Chaiyen, P.; Diederich, F. Antimalarial Inhibitors Targeting Serine Hydroxymethyltransferase (SHMT) with in Vivo Efficacy and Analysis of their Binding Mode Based on X-ray Cocrystal Structures. *J. Med. Chem.* **2017**, *60*, 4840−4860.

(7) Schwertz, G.; Frei, M. S.; Witschel, M. C.; Rottmann, M.; Leartsakulpanich, U.; Chitnumsub, P.; Jaruwat, A.; Ittarat, W.; Schafer, A.; Aponte, R. A.; Trapp, N.; Mark, K.; Chaiyen, P.; Diederich, F. Conformational Aspects in the Design of Inhibitors for Serine Hydroxymethyltransferase (SHMT): Biphenyl, Aryl Sulfonamide, and Aryl Sulfone Motifs. *Chem. - Eur. J.* **2017**, *23*, 14345−14357.

(8) Pornthanakasem, W.; Kongkasuriyachai, D.; Uthaipibull, C.; Yuthavong, Y.; Leartsakulpanich, U. Plasmodium serine hydroxymethyltransferase: indispensability and display of distinct localization. *Malar. J.* **2012**, *11*, 387.

(9) Newman, A. C.; Maddocks, O. D. K. One-carbon metabolism in cancer. *Br. J. Cancer* **2017**, *116*, 1499.

(10) Franca, T. C.; Pascutti, P. G.; Ramalho, T. C.; Figueroa-Villar, J. D. A three-dimensional structure of Plasmodium falciparum serine hydroxymethyltransferase in complex with glycine and 5-formyl-tetrahydrofolate. Homology modeling and molecular dynamics. *Biophys. Chem.* **2005**, *115*, 1−10.

(11) Cerqueira, N. M.; Fernandes, P. A.; Ramos, M. J. Computational Mechanistic Studies Addressed to the Transimination Reaction Present in All Pyridoxal 5′-Phosphate-Requiring Enzymes. *J. Chem. Theory Comput.* **2011**, *7*, 1356−68.

(12) Oliveira, E. F.; Cerqueira, N. M.; Fernandes, P. A.; Ramos, M. J. Mechanism of formation of the internal aldimine in pyridoxal 5′-phosphate-dependent enzymes. *J. Am. Chem. Soc.* **2011**, *133*, 15496−505.

(13) Florio, R.; Chiaraluce, R.; Consalvi, V.; Paiardini, A.; Catacchio, B.; Bossa, F.; Contestabile, R. The role of evolutionarily conserved hydrophobic contacts in the quaternary structure stability of Escherichia coli serine hydroxymethyltransferase. *FEBS J.* **2009**, *276*, 132−43.

(14) Angelaccio, S.; di Salvo, M. L.; Parroni, A.; Di Bello, A.; Contestabile, R.; Pascarella, S. Structural stability of cold-adapted serine hydroxymethyltransferase, a tool for β-hydroxy-α-amino acid biosynthesis. *J. Mol. Catal. B: Enzym.* **2014**, *110*, 171−177.

(15) Schirch, V.; Szebenyi, D. M. Serine hydroxymethyltransferase revisited. *Curr. Opin. Chem. Biol.* **2005**, *9*, 482−7.

(16) Szebenyi, D. M.; Musayev, F. N.; di Salvo, M. L.; Safo, M. K.; Schirch, V. Serine hydroxymethyltransferase: role of glu75 and evidence that serine is cleaved by a retroaldol mechanism. *Biochemistry* **2004**, *43*, 6865−76.

(17) Scarsdale, J. N.; Radaev, S.; Kazanina, G.; Schirch, V.; Wright, H. T. Crystal structure at 2.4 Å resolution of E. coli serine hydroxymethyltransferase in complex with glycine substrate and 5-formyl tetrahydrofolate11Edited by I. A. Wilson. *J. Mol. Biol.* **2000**, *296*, 155−168.

(18) Rao, J. V.; Prakash, V.; Rao, N. A.; Savithri, H. S. The role of Glu74 and Tyr82 in the reaction catalyzed by sheep liver cytosolic serine hydroxymethyltransferase. *Eur. J. Biochem.* **2000**, *267*, 5967−76.

(19) Kallen, R. G.; Jencks, W. P. The mechanism of the condensation of formaldehyde with tetrahydrofolic acid. *J. Biol. Chem.* **1966**, *241*, 5851−5863.

(20) Chitnumsub, P.; Ittarat, W.; Jaruwat, A.; Noytanom, K.; Amornwatcharapong, W.; Pornthanakasem, W.; Chaiyen, P.; Yuthavong, Y.; Leartsakulpanich, U. The structure of Plasmodium falciparum serine hydroxymethyltransferase reveals a novel redox switch that regulates its activities. *Acta Crystallogr., Sect. D: Biol. Crystallogr.* **2014**, *70*, 1517−1527.

(21) Altschul, S. F.; Madden, T. L.; Schaffer, A. A.; Zhang, J.; Zhang, Z.; Miller, W.; Lipman, D. J. Gapped BLAST and PSI-BLAST: a new generation of protein database search programs. *Nucleic Acids Res.* **1997**, *25*, 3389−3402.

(22) Altschul, S. F.; Wootton, J. C.; Gertz, E. M.; Agarwala, R.; Morgulis, A.; Schaffer, A. A.; Yu, Y. K. Protein database searches using compositionally adjusted substitution matrices. *FEBS J.* **2005**, *272*, 5101−9.

(23) Frisch, M. J.; Trucks, G. W.; Schlegel, H. B.; Scuseria, G. E.; Robb, M. A.; Cheeseman, J. R.; Scalmani, G.; Barone, V.; Mennucci, B.; Petersson, G. A.; Nakatsuji, H.; Caricato, M.; Li, X.; Hratchian, H. P.; Izmaylov, A. F.; Bloino, J.; Zheng, G.; Sonnenberg, J. L.; Hada, M.; Ehara, M.; Toyota, K.; Fukuda, R.; Hasegawa, J.; Ishida, M.; Nakajima, T.; Honda, Y.; Kitao, O.; Nakai, H.; Vreven, T.; Montgomery, J. A., Jr.; Peralta, J. E.; Ogliaro, F.; Bearpark, M. J.; Heyd, J.; Brothers, E. N.; Kudin, K. N.; Staroverov, V. N.; Kobayashi, R.; Normand, J.; Raghavachari, K.; Rendell, A. P.; Burant, J. C.; Iyengar, S. S.; Tomasi, J.; Cossi, M.; Rega, N.; Millam, N. J.; Klene, M.; Knox, J. E.; Cross, J. B.; Bakken, V.; Adamo, C.; Jaramillo, J.; Gomperts, R.; Stratmann, R. E.; Yazyev, O.; Austin, A. J.; Cammi, R.; Pomelli, C.; Ochterski, J. W.; Martin, R. L.; Morokuma, K.; Zakrzewski, V. G.; Voth, G. A.; Salvador, P.; Dannenberg, J. J.; Dapprich, S.; Daniels, A. D.; Farkas, Ö.; Foresman, J. B.; Ortiz, J. V.; Cioslowski, J.; Fox, D. J. *Gaussian 09*; Gaussian, Inc.: Wallingford, CT, USA, 2009.

(24) Mahoney, M. W.; Jorgensen, W. L. A five-site model for liquid water and the reproduction of the density anomaly by rigid,

DOI: 10.1021/acscatal.8b02321
ACS Catal. 2018, 8, 10096−10110

nonpolarizable potential functions. *J. Chem. Phys.* **2000**, *112*, 8910−8922.
(25) Case, D. A.; Darden, T. A.; Cheatham, T. E.; Simmerling, C. L.; Wang, J.; Duke, R. E.; Luo, R.; Walker, R. C.; Zhang, W.; Merz, K. M.; Roberts, B.; Hayik, S.; Roitberg, A.; Seabra, G.; Swails, J.; Goetz, A. W.; Kolossváry, I.; Wong, K. F.; Paesani, F.; Vanicek, J.; Wolf, R. M.; Liu, J.; Wu, X.; Brozell, S. R.; Steinbrecher, T.; Gohlke, H.; Cai, Q.; Ye, X.; Wang, J.; Hsieh, M. J.; Cui, G.; Roe, D. R.; Mathews, D. H.; Seetin, M. G.; Salomon-Ferrer, R.; Sagui, C.; Babin, V.; Luchko, T.; Gusarov, S.; Kovalenko, A.; Kollman, P. A. *AMBER 12*; University of California: San Francisco, CA, 2012.
(26) Sondergaard, C. R.; Olsson, M. H.; Rostkowski, M.; Jensen, J. H. Improved Treatment of Ligands and Coupling Effects in Empirical Calculation and Rationalization of pKa Values. *J. Chem. Theory Comput.* **2011**, *7*, 2284−95.
(27) Olsson, M. H.; Sondergaard, C. R.; Rostkowski, M.; Jensen, J. H. PROPKA3: Consistent Treatment of Internal and Surface Residues in Empirical pKa Predictions. *J. Chem. Theory Comput.* **2011**, *7*, 525−37.
(28) Wang, J.; Wolf, R. M.; Caldwell, J. W.; Kollman, P. A.; Case, D. A. Development and testing of a general amber force field. *J. Comput. Chem.* **2004**, *25*, 1157−74.
(29) Hornak, V.; Abel, R.; Okur, A.; Strockbine, B.; Roitberg, A.; Simmerling, C. Comparison of multiple Amber force fields and development of improved protein backbone parameters. *Proteins: Struct., Funct., Genet.* **2006**, *65*, 712−25.
(30) Fernandes, H. S.; Ramos, M. J.; Cerqueira, N. M. F. S. A. molUP: A VMD plugin to handle QM and ONIOM calculations using the gaussian software. *J. Comput. Chem.* **2018**, *39*, 1344−1353.
(31) Humphrey, W.; Dalke, A.; Schulten, K. VMD: visual molecular dynamics. *J. Mol. Graphics* **1996**, *14*, 33−38.
(32) Cerqueira, N.; Fernandes, P. A.; Ramos, M. J. Protocol for Computational Enzymatic Reactivity Based on Geometry Optimisation. *ChemPhysChem* **2018**, *19*, 669−689.
(33) Dapprich, S.; Komaromi, I.; Byun, K. S.; Morokuma, K.; Frisch, M. J. A new ONIOM implementation in Gaussian98. Part I. The calculation of energies, gradients, vibrational frequencies and electric field derivatives. *J. Mol. Struct.: THEOCHEM* **1999**, *461-462*, 1−21.
(34) Svensson, M.; Humbel, S.; Froese, R. D. J.; Matsubara, T.; Sieber, S.; Morokuma, K. ONIOM: A Multilayered Integrated MO + MM Method for Geometry Optimizations and Single Point Energy Predictions. A Test for Diels−Alder Reactions and Pt(P(t-Bu)3)2 + H2 Oxidative Addition. *J. Phys. Chem.* **1996**, *100*, 19357−19363.
(35) Maseras, F.; Morokuma, K. IMOMM: A new integrated ab initio + molecular mechanics geometry optimization scheme of equilibrium structures and transition states. *J. Comput. Chem.* **1995**, *16*, 1170−1179.
(36) Yanai, T.; Tew, D. P.; Handy, N. C. A new hybrid exchange−correlation functional using the Coulomb-attenuating method (CAM-B3LYP). *Chem. Phys. Lett.* **2004**, *393*, 51−57.
(37) Fernandes, H. S.; Ramos, M. J.; Cerqueira, N. The Catalytic Mechanism of the Pyridoxal-5′-phosphate-Dependent Enzyme, Histidine Decarboxylase: A Computational Study. *Chem. - Eur. J.* **2017**, *23*, 9162−9173.
(38) Ribeiro, A. J. M.; Santos-Martins, D.; Russo, N.; Ramos, M. J.; Fernandes, P. A. Enzymatic Flexibility and Reaction Rate: A QM/MM Study of HIV-1 Protease. *ACS Catal.* **2015**, *5*, 5617−5626.
(39) Oliveira, E. F.; Cerqueira, N. M. F. S. A.; Ramos, M. J.; Fernandes, P. A. QM/MM study of the mechanism of reduction of 3-hydroxy-3-methylglutaryl coenzyme A catalyzed by human HMG-CoA reductase. *Catal. Sci. Technol.* **2016**, *6*, 7172−7185.
(40) Neves, R. P. P.; Fernandes, P. A.; Ramos, M. J. Unveiling the Catalytic Mechanism of NADP+-Dependent Isocitrate Dehydrogenase with QM/MM Calculations. *ACS Catal.* **2016**, *6*, 357−368.
(41) Moreira, C.; Ramos, M. J.; Fernandes, P. A. Reaction Mechanism of Mycobacterium Tuberculosis Glutamine Synthetase Using Quantum Mechanics/Molecular Mechanics Calculations. *Chem. - Eur. J.* **2016**, *22*, 9218−9225.
(42) Gesto, D. S.; Cerqueira, N. M. F. S. A.; Fernandes, P. A.; Ramos, M. J. Unraveling the enigmatic mechanism of l-asparaginase II with QM/QM calculations. *J. Am. Chem. Soc.* **2013**, *135*, 7146−7158.
(43) Cerqueira, N. M. F. S. A.; Gonzalez, P. J.; Fernandes, P. A.; Moura, J. J. G.; Ramos, M. J. Periplasmic Nitrate Reductase and Formate Dehydrogenase: Similar Molecular Architectures with Very Different Enzymatic Activities. *Acc. Chem. Res.* **2015**, *48*, 2875−2884.
(44) Cassimjee, K. E.; Manta, B.; Himo, F. A quantum chemical study of the omega-transaminase reaction mechanism. *Org. Biomol. Chem.* **2015**, *13*, 8453−64.
(45) Fukui, K. The path of chemical reactions - the IRC approach. *Acc. Chem. Res.* **1981**, *14*, 363−368.
(46) Riplinger, C.; Neese, F. An efficient and near linear scaling pair natural orbital based local coupled cluster method. *J. Chem. Phys.* **2013**, *138*, 034106.
(47) Riplinger, C.; Sandhoefer, B.; Hansen, A.; Neese, F. Natural triple excitations in local coupled cluster calculations with pair natural orbitals. *J. Chem. Phys.* **2013**, *139*, 134101.
(48) Liakos, D. G.; Sparta, M.; Kesharwani, M. K.; Martin, J. M.; Neese, F. Exploring the Accuracy Limits of Local Pair Natural Orbital Coupled-Cluster Theory. *J. Chem. Theory Comput.* **2015**, *11*, 1525−39.
(49) Liakos, D. G.; Neese, F. Is It Possible To Obtain Coupled Cluster Quality Energies at near Density Functional Theory Cost? Domain-Based Local Pair Natural Orbital Coupled Cluster vs Modern Density Functional Theory. *J. Chem. Theory Comput.* **2015**, *11*, 4054−63.
(50) Sparta, M.; Neese, F. Chemical applications carried out by local pair natural orbital based coupled-cluster methods. *Chem. Soc. Rev.* **2014**, *43*, 5032−41.
(51) Paiva, P.; Sousa, S. F.; Ramos, M. J.; Fernandes, P. A. Understanding the Catalytic Machinery and the Reaction Pathway of the Malonyl-Acetyl Transferase Domain of Human Fatty Acid Synthase. *ACS Catal.* **2018**, *8*, 4860−4872.
(52) Bistoni, G.; Polyak, I.; Sparta, M.; Thiel, W.; Neese, F. Towards accurate QM/MM reaction barriers with large QM regions using Domain Based Pair Natural Orbital Coupled Cluster Theory. *J. Chem. Theory Comput.* **2018**, *14*, 3524−3531.
(53) Neese, F. Software update: the ORCA program system, version 4.0. *Wiley Interdiscip. Rev.: Comput. Mol. Sci.* **2018**, *8*, e1327.
(54) Dunning, T. H., Jr Gaussian basis sets for use in correlated molecular calculations. I. The atoms boron through neon and hydrogen. *J. Chem. Phys.* **1989**, *90*, 1007−1023.
(55) Hättig, C. Optimization of auxiliary basis sets for RI-MP2 and RI-CC2 calculations: Core−valence and quintuple-ζ basis sets for H to Ar and QZVPP basis sets for Li to Kr. *Phys. Chem. Chem. Phys.* **2005**, *7*, 59−66.
(56) Weigend, F.; Köhn, A.; Hättig, C. Efficient use of the correlation consistent basis sets in resolution of the identity MP2 calculations. *J. Chem. Phys.* **2002**, *116*, 3175−3183.
(57) Truhlar, D. G. Basis-set extrapolation. *Chem. Phys. Lett.* **1998**, *294*, 45−48.
(58) Ngo, H. P.; Cerqueira, N. M.; Kim, J. K.; Hong, M. K.; Fernandes, P. A.; Ramos, M. J.; Kang, L. W. PLP undergoes conformational changes during the course of an enzymatic reaction. *Acta Crystallogr., Sect. D: Biol. Crystallogr.* **2014**, *70*, 596−606.
(59) Dunathan, H. C. Stereochemical aspects of pyridoxal phosphate catalysis. *Adv. Enzymol. Relat. Areas Mol. Biol.* **2006**, *35*, 79−134.
(60) Di Salvo, M. L.; Scarsdale, J. N.; Kazanina, G.; Contestabile, R.; Schirch, V.; Wright, H. T. Structure-based mechanism for early PLP-mediated steps of rabbit cytosolic serine hydroxymethyltransferase reaction. *BioMed Res. Int.* **2013**, *2013*, 458571.
(61) Jain, M.; Nilsson, R.; Sharma, S.; Madhusudhan, N.; Kitami, T.; Souza, A. L.; Kafri, R.; Kirschner, M. W.; Clish, C. B.; Mootha, V. K. Metabolite Profiling Identifies a Key Role for Glycine in Rapid Cancer Cell Proliferation. *Science* **2012**, *336*, 1040−1044.
(62) Dunathan, H. C. Conformation and reaction specificity in pyridoxal phosphate enzymes. *Proc. Natl. Acad. Sci. U. S. A.* **1966**, *55*, 712−6.

DOI: 10.1021/acscatal.8b02321
ACS Catal. 2018, 8, 10096−10110